JOURNAL OF GEOPHYSICAL RESEARCH, VOL. 117, B10102, doi:10.1029/2012JB009349, 2012

3-D focused inversion of near-seafloor magnetic data with application to the Brothers volcano hydrothermal system, Southern Pacific Ocean, New Zealand

F. Caratori Tontini,[1] C. E. J. de Ronde,[1] D. Yoerger,[2] J. Kinsey,[2] and M. Tivey[2]

Received 29 March 2012; revised 26 August 2012; accepted 4 September 2012; published 11 October 2012.

[1] We describe and apply a new inversion method for 3-D modeling of magnetic anomalies designed for general application but which is particularly useful for the interpretation of near-seafloor magnetic anomalies. The crust subsurface is modeled by a set of prismatic cells, each with uniform magnetization, that together reproduce the observed magnetic field. This problem is linear with respect to the magnetization, and the number of cells is normally greater than the amount of available data. Thus, the solution is obtained by solving an under-determined linear problem. A focused solution, exhibiting sharp boundaries between different magnetization domains, is obtained by allowing the amplitudes of magnetization to vary between a pre-determined range and by minimizing the region of the 3-D space where the source shows large variations, i.e., large gradients. A regularization functional based on a depth-weighting function is also introduced in order to counter-act the natural decay of the magnetic field intensity with depth. The inversion method has been used to explore the characteristics of the submarine hydrothermal system of Brothers volcano in the Kermadec arc, by inverting near-bottom magnetic data acquired by Autonomous Underwater Vehicles (AUVs). Different surface expressions of the hydrothermal vent fields show specific vertical structures in their underlying demagnetization regions that we interpret to represent hydrothermal upflow zones. For example, at focused vent sites the demagnetized conduits are vertical, pipe-like structures extending to depths of ~1000 m below the seafloor, whereas at diffuse vent sites the demagnetization regions are characterized by thin and inclined conduits.

Citation: Caratori Tontini, F., C. E. J. de Ronde, D. Yoerger, J. Kinsey, and M. Tivey (2012), 3-D focused inversion of near-seafloor magnetic data with application to the Brothers volcano hydrothermal system, Southern Pacific Ocean, New Zealand, *J. Geophys. Res.*, *117*, B10102, doi:10.1029/2012JB009349.

1. Introduction

[2] Quantitative interpretation of potential-field data, focused on the stable estimation of key physical source parameters (e.g., density or magnetization) from a measured set of observations, is an inverse problem. Forward equations relating source parameters to observations are not analytically invertible, and it is impossible to obtain a unique 3-D model of the generating source from the limited amount of observations. Geophysical inverse problems are, in effect, characterized by ambiguities and instabilities of their solutions [*Tikhonov and Arsenin*, 1977; *Tarantola*, 1987; *Menke*, 1989].

[3] The most challenging problem, therefore, deals with theoretical non-uniqueness. This problem has been known since Gauss' time and is a consequence of potential-field data being harmonic and therefore obeying the Laplace equation. For any known harmonic field on a closed surface there is an infinite set of equivalent sources within that surface that generate exactly the same field [*Blakely*, 1995]. In other words, it is theoretically possible to find a non-trivial magnetization, or density distribution, that produces an exact null field on a given observation surface. As a proof of non-uniqueness, this particular distribution, also known as the annihilator [*Parker and Huestis*, 1974], can be added to any particular generating source without changing the corresponding field.

[4] Algebraic ambiguity is another problem, which derives from the limited accuracy of potential-field surveys that provide information by a finite number of discrete observations. Using a linear approach, the number of parameters required to recover a full 3-D model of the generating source is large, in comparison with the available observations. Although the relation between parameters and observations is linear, the matrix implementing this linear relationship is rank-deficient and has a significant null-space, i.e., is characterized by a large number of linearly dependent rows (or columns).

[5] A further term of non-uniqueness derives from experimental problems, i.e., it comes from geological, or experimental noise in the data that may affect the resolution of the

[1]GNS Science, Lower Hutt, New Zealand.
[2]Woods Hole Oceanographic Institution, Woods Hole, Massachusetts, USA.

Corresponding author: F. Caratori Tontini, GNS Science, 1 Fairway Dr., Lower Hutt 5010, New Zealand. (f.caratori.tontini@gns.cri.nz).

0148-0227/12/2012JB009349

model. Again, there is more than one solution which may fit the noisy observations within the same degree of accuracy. The most obvious consequence of these ambiguities is that an optimal solution, subject to fitting the observation, can be found for any given depth-range. For this reason, inverse modeling without external constraints commonly yields shallow solutions because they also represent the minimum-norm solution in a least squares sense [*Li and Oldenburg*, 1996].

[6] In effect, potential-field ambiguities can be reduced by introducing some "a priori" information about the source geometry in order to obtain a unique solution subject to fitting the observations and satisfying some basic properties regarding the model shape. This is typically achieved by subdividing the Earth's subsurface/subseafloor into a mesh of prismatic cells (also known as voxels, or volume pixels), characterized by constant densities or magnetizations, where the inversion provides the values for these parameters. This parameter estimation is obtained by minimizing an objective functional that consists of a misfit term and a regularization term. The former is responsible for fitting the observation, for example in a least squares sense, whereas the latter optimizes the model characteristics according to the imposed "a priori" information. This regularization procedure is equivalent to the statistical (Bayesian) inversion approach [*Ho-Liu et al.*, 1989; *Yanovskaya and Ditmar*, 1990; *Simons et al.*, 2002].

[7] Several methods have been proposed by previous authors in order to regularize the inverse problem and obtain a meaningful solution; a review of some of the existing methods is given in *Boulanger and Chouteau* [2001] and *Silva et al.* [2001]. Compactness of the solution is one of the widely imposed constraints in the regularized solution. Spreading of the source can be reduced by minimizing the total volume [*Last and Kubik*, 1983], or the moment of inertia [*Guillen and Menichetti*, 1984] of the source. Compactness can be imposed along different axes by incorporating information about the axis length [*Barbosa and Silva*, 1994]. Compactness can also be obtained by describing the source geometry by a set of positively constrained 3-D Gaussian functions [*Caratori Tontini et al.*, 2003].

[8] *Li and Oldenburg* [1996] were the first to propose the use of a depth-weighting function to counteract the natural decay of potential-fields with depth, by giving increasing weights to voxels at greater depths. The idea of a depth-weighting function has since been successively incorporated into several inversion algorithms [e.g., *Pilkington*, 1997; *Boulanger and Chouteau*, 2001; *Caratori Tontini et al.*, 2006; *Cella and Fedi*, 2012], providing meaningful results.

[9] The regularization functional has the important property of producing a stable solution, which is usually obtained by maximum smoothness criteria. In this case, the mathematical formulation of the inverse problem is simplified by requiring the solution to be as smooth as possible. However, subsurface geology is commonly characterized by sharp boundaries and therefore smooth solutions do not readily resolve the discontinuities between different geological formations. In order to solve this problem, *Portniaguine and Zhdanov* [2002] proposed the use of a minimum support stabilizing functional that has the relevant property of focusing the inverse solution, and thus producing sharp boundaries [*Zhdanov*, 2002].

[10] Here, we propose a modification of the inversion strategy developed by *Portniaguine and Zhdanov* [2002]. The algorithm is of general application although it is especially designed to invert near-seafloor magnetic data above submarine volcanoes. To this aim, we first introduce a topographic constraint to the inversion model, i.e., the voxels lying outside of the topographical relief are removed. An inequality constraint is then used in order to bound the magnetization values to lie within a predetermined range. Next, a focused solution is obtained by minimizing a regularization functional based on the volume of the subsurface region where the model exhibits strong variations. This regularization is achieved through the use of gradients of the magnetization distribution. A depth-weighting function adapted from *Li and Oldenburg* [1996] is also included to provide equal sensitivity to cells located at different depths.

[11] In the following sections we describe the mathematical formulation of the inversion method and its performance by applying it to a synthetic uniform magnetization model for Brothers volcano, north of North Island, New Zealand (Figure 1). Thereafter, the inversion of near-bottom magnetic data collected by Autonomous Underwater Vehicles (AUVs) shows the implications for 3-D structures related to the Brothers volcano subseafloor hydrothermal system. This is because magnetic anomaly data provide important information about the characteristics of submarine hydrothermal systems as hydrothermal processes can destroy the magnetization of volcanic rocks [*Tivey and Dyment*, 2010]. If the volume of hydrothermal alteration is large and/or the depth of the hydrothermal system is shallow, the corresponding reduced magnetization regions can be detected by surface ship-borne data [*Cocchi et al.*, 2009; *Caratori Tontini et al.*, 2009, 2010]. However, for depths greater than ~1 km, surface magnetic data lack the resolution required to map the geometry of hydrothermal systems in detail. AUVs are excellent tools to achieve this level of resolution in the submarine environment as they fill the gap in scale between surface ship-borne data and local information obtained from manned submersibles and/or remotely operated vehicles.

[12] Brothers volcano is one of the most hydrothermally active volcanoes found along the Kermadec arc, and its large hydrothermal system is characterized by different vent fields with individual characteristics and manifestations of hydrothermal activity on the seafloor [*de Ronde et al.*, 2005, 2011]. Here, we will show in particular how the subsurface 3-D magnetization distribution correlates with different vent fields characteristics at focused and diffuse sites.

2. Geological and Geophysical Setting of Brothers Volcano

[13] Brothers volcano is located along the 2500 km long Kermadec intraoceanic arc (Figure 1), formed by the subduction of the Pacific plate beneath the Australian plate [*de Ronde et al.*, 2001, 2007, 2011]. The age of Brothers volcanism is not clearly defined, but limited K-Ar dating [*Wright*, 1994] and aeromagnetic anomaly data [*Malahoff et al.*, 1982] suggest that Brothers volcano is younger than 0.78 Ma. Brothers volcano covers an approximate area of 13×8 km^2, with a 3 km wide caldera surrounded by 300–500 m high walls (Figure 1). The volcano morphology is characterized by several NE-SW lineaments that may

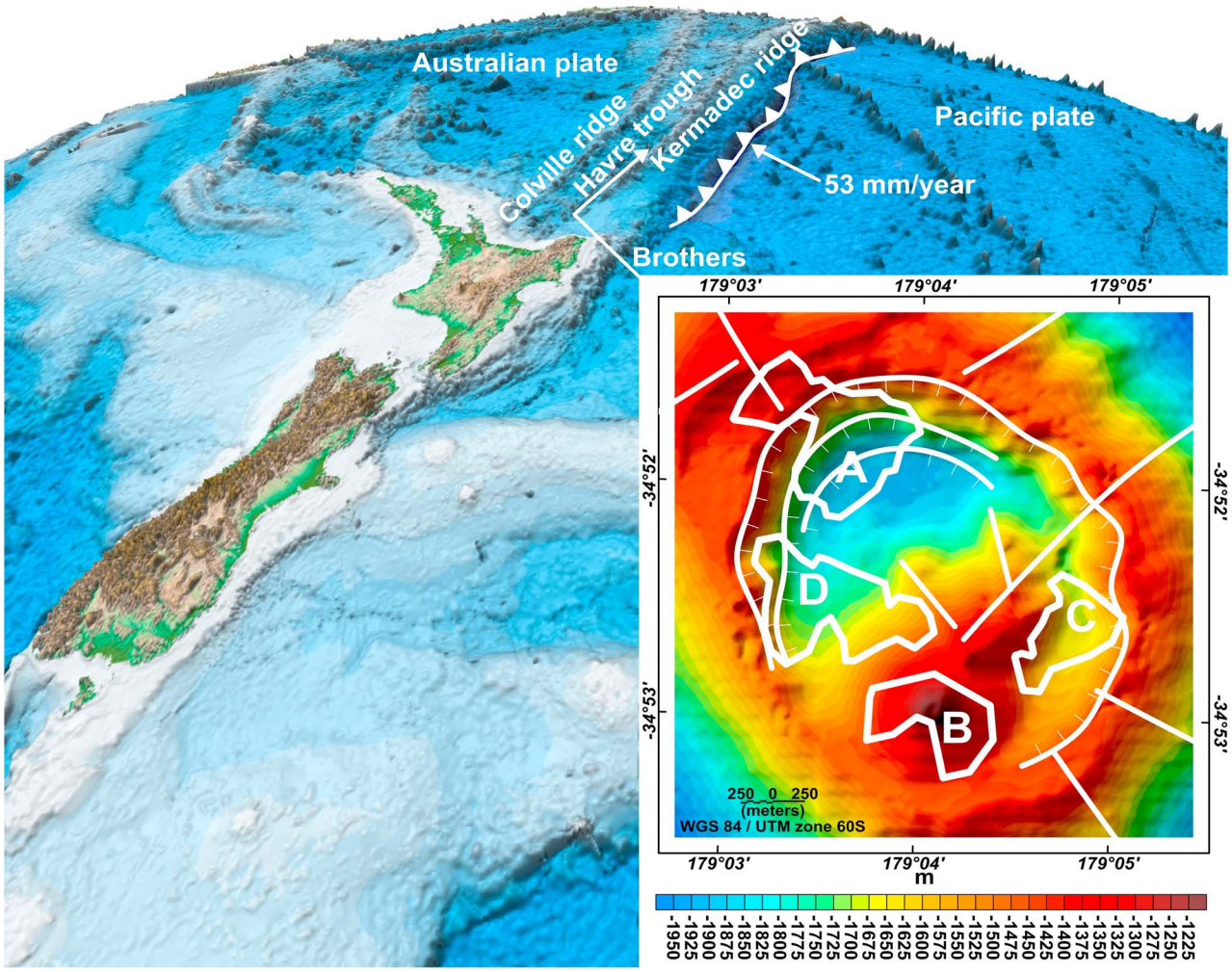

Figure 1. Brothers volcano location and tectonic setting. Subduction rate from *DeMets et al.* [2010]. Inset shows Brothers volcano bathymetry, with locations of known hydrothermal vent sites (A–D), structural lineaments and ring faults: A, NW caldera site; B, Cone site; C, SE caldera site; D, W caldera site. Sites A and D are focused sites, whereas B and C are diffuse. Active venting has been visually observed at sites A and B.

represent the surface expressions of large, subduction-related, regional faults [*Embley et al.*, 2012].

[14] The location of some of the known hydrothermal fields (i.e., areas A, B, C, D in Figure 1) at Brothers is correlated with the caldera faults [*de Ronde et al.*, 2005]. Dredged sulfide samples [*Wright et al.*, 1998; *de Ronde et al.*, 2005], plume mapping cruises [*de Ronde et al.*, 2001, 2007], and subsequent detailed mapping by manned submersible dives, camera tows and AUV dives [*de Ronde et al.*, 2011; *Caratori Tontini et al.*, 2012; *Embley et al.*, 2012; *Baker et al.*, 2012] between 1996 and 2011 have located four separate hydrothermal vent fields: three of them (A,C, and D) form a donut-like pattern along the caldera walls and a fourth one (B) is perched atop the volcanic cone inside the caldera (Figure 1). The boundaries and locations of the four known hydrothermal vent fields at Brothers were inferred by combining the results of the magnetic study in *Caratori Tontini et al.* [2012] with previously available information derived from seafloor observations using towed cameras, submersible dives and hydrothermal plume mapping. A further differentiation between diffuse and focused vent sites can be derived at Brothers volcano.

[15] Diffuse sites are characterized by consistent mixings of the hydrothermal fluids with cold seawater during their ascent to the seafloor, with low-temperature vents (<200°), whereas focused sites are characterized by well-sealed upflow zones, with high-temperature vents forming sulfide chimneys and black smokers. At Brothers volcano, diffuse venting occurs at the cone (B in Figure 1) and the East caldera fields (C in Figure 1), whereas focused venting has been observed at the NW caldera (A in Figure 1) and the West caldera (D in Figure 1) fields [*Baker et al.*, 2012; *de Ronde et al.*, 2011]. Acoustic tremor data derived from Ocean Bottom Hydrophones (OBHs), located inside the caldera, show a large number of hydrothermal fluid conduits/chambers in the southern sector of Brothers volcano, and the top of a magma chamber at a depth of ~3.7 km, i.e. about 2.5 km beneath the cone [*Dziak et al.*, 2008; *de Ronde et al.*, 2011].

[16] Detailed, near-bottom surveys of Brothers volcano were performed by AUVs. During the 2007 ROVARK

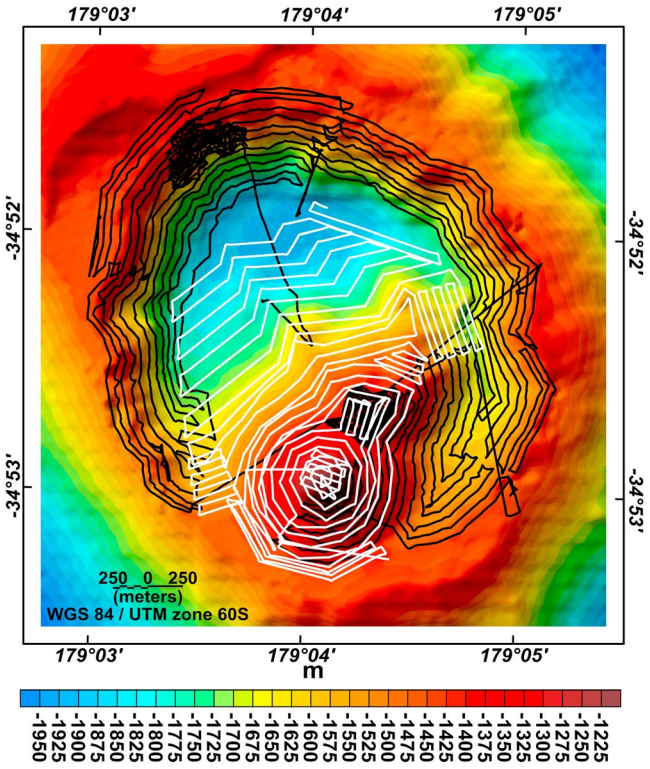

Figure 2. Survey geometry by *ABE* (black tracklines) and *Sentry* (white tracklines). Survey altitude above the volcano topography was 50 m.

cruise [*Merle et al.*, 2007], the *ABE* (Authonomous Benthic Explorer) AUV of the Woods Hole Oceanographic Institution (WHOI) was deployed from the German R/V *Sonne* to survey the caldera walls and the cone. The caldera floor was later re-surveyed by the AUV *Sentry* of WHOI during the 2011 NZASMS cruise. *ABE* and *Sentry* were both equipped with CTDs and optical backscatter, pH and Eh sensors, and fluxgate magnetometers, in addition to multibeam (*ABE*) and side scan sonar (*Sentry*). The AUVs were programmed to fly at an altitude of ∼50 m above the seafloor, with undulations from this draped surface less than ±20 m. The combined surveys consisted of ∼220 km of track lines with an average line-spacing of 50 m (Figure 2). The magnetic data collected during these surveys were corrected for remanent and induced magnetic noise derived from the AUV [*Caratori Tontini et al.*, 2012], by fitting the sinusoidal variation of the magnetic field data while the AUV spins during its descent/ascent to/from the seafloor [*Tivey et al.*, 2003]. The total-intensity anomaly field (Figure 3) was obtained by subtracting the International Geomagnetic Reference Field (IGRF) from the total-field magnetic data [*Finlay et al.*, 2010]. Magnetic data recorded at the Eyrewell Intermagnet observatory (Christchurch, New Zealand) show that the Brothers volcano survey was performed during magnetically quiet days. Diurnal variations were not subtracted from the recorded data because a base station could not be operated for logistical reasons [*Faggioni and Caratori Tontini*, 2003]. Comparing our measured anomalies with the Eyrewell Intermagnet observatory data, it is clear that crustal anomalies at Brothers volcano are large relative to diurnal effects.

[17] The survey geometry and the magnetic data processing is described in detail elsewhere [*Caratori Tontini et al.*, 2012], where the magnetic anomaly data were interpreted by a 2D inversion method to obtain an equivalent horizontal magnetization distribution that correlated with the seafloor expression of the hydrothermal vent fields. The inversion was based on a magnetized layer with vertically invariant magnetization enclosed by a top surface defined by the seafloor surface and a bottom layer fixed at a constant basal depth of 2500 m, consistent with the seafloor surrounding the volcano. The corresponding magnetization distribution (Figure 4) does not vary vertically and is therefore most representative of the shallow surface expressions of the variation in magnetization. Here, we combine and discuss this information with the results obtained from the 3-D inversion of the Brothers magnetic data. The 3-D inversion model shows variations in the subseafloor magnetization that can be correlated with the subsurface structure of the hydrothermal upflow zones.

3. Inversion Strategy

[18] We have n observations of magnetic field variation organized in the data vector **d**. The observations can be scattered and/or collected at variable altitudes above the topography/seafloor. We then subdivide the subsurface into a set of small rectangular cells, further assuming that these cells have uniform magnetization (Figure 5). At this point, we use a bathymetric model to remove the cells lying above the seafloor relief. This procedure is particularly useful in

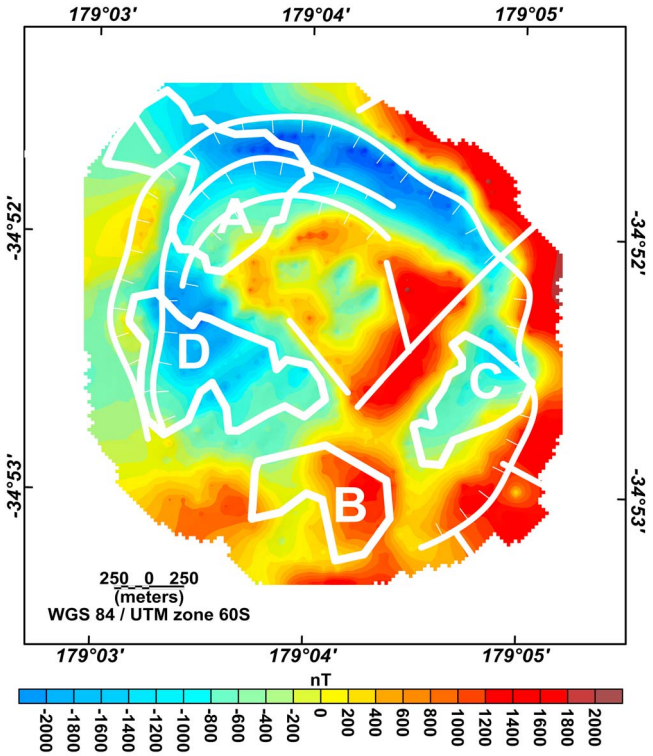

Figure 3. Brothers volcano magnetic anomaly (total-intensity) measured by AUVs, redrawn from [*Caratori Tontini et al.*, 2012]. Hydrothermal vent sites, structural lineaments and ring faults described in Figure 1.

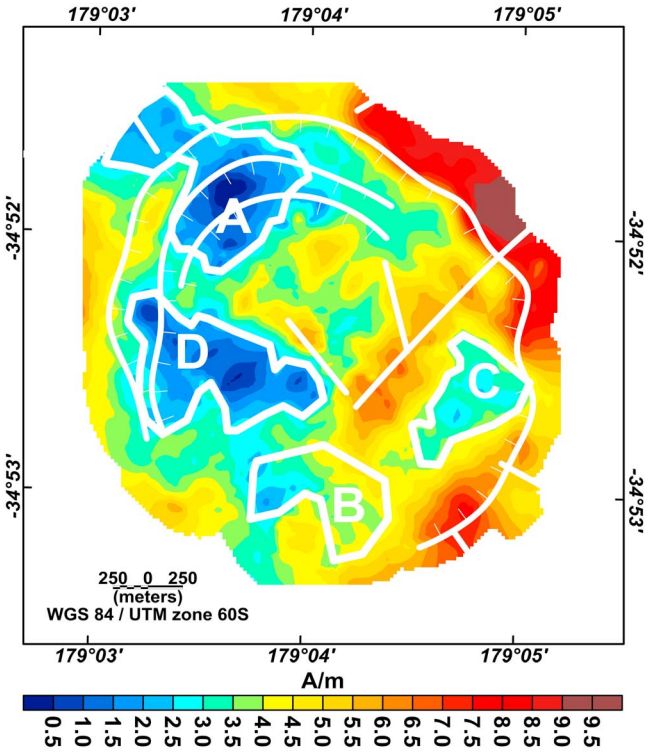

Figure 4. Brothers volcano apparent magnetization map, redrawn from *Caratori Tontini et al.* [2012]. Hydrothermal vent sites, structural lineaments and ring faults described in Figure 1. Very low magnetizations are visible at the focused NW caldera and W caldera (sites A and B). Less reduced magnetizations zones are still visible at the diffuse cone and SE caldera (sites C and D).

reducing the number of free parameters, especially when studying submarine volcanoes, which are characterized by uneven topographies. The remaining m magnetization parameters are then grouped into a vector $\mathbf{p}$. The aim of the inversion therefore is to obtain the elements of the vector $\mathbf{p}$ from the observations $\mathbf{d}$, i.e., the magnetization from the observed anomaly data. The relationship between these quantities is linear and can be expressed by an $n \times m$ kernel matrix $\mathbf{K}$ as shown by the following equation

$$\mathbf{d} = \mathbf{K} \cdot \mathbf{p}. \tag{1}$$

The indexes i, j of the matrix $\mathbf{K}_{ij}$ represent the contribution given by the jth cell of the mesh to the ith observation, respectively (Figure 5). The matrix $\mathbf{K}$ is obtained by using the forward equations of *Bhattacharyya* [1964], who derived the analytical expression of the magnetic field generated by a prismatic source. The kernel matrix is characterized by decreasing values at increasing depths of the cells because the magnetic field falls off as r^{-3}, where r is the spatial distance between source and observation. This natural decay generates small magnetization values in a free inversion, especially in the shallow layers. To counteract this effect and give equal weight to cells at different depths, we introduce a depth-weighting function [*Li and Oldenburg*, 1996] in the form of a multiplying matrix $\mathbf{W}$ [*Caratori Tontini et al.*, 2006].

This multiplying matrix is an $m \times m$ matrix containing the correction terms z^3 for each cell of the mesh, z in this case being the vertical distance between the observation elevation and the cell center. If the magnetic source is characterized by a specific structural index, the cubic exponent should be changed according to the structural index exponent [*Cella and Fedi*, 2012]. Equation (1) becomes

$$\mathbf{d} = \mathbf{K} \cdot \mathbf{W} \cdot \mathbf{W}^{-1} \cdot \mathbf{p}, \tag{2}$$

and by introducing the weighted kernel matrix

$$\mathbf{K}^w = \mathbf{K} \cdot \mathbf{W}, \tag{3}$$

we can invert the revised equation

$$\mathbf{d} = \mathbf{K}^w \cdot \mathbf{p}^w, \tag{4}$$

for the weighted vector $\mathbf{p}^w$

$$\mathbf{p}_w = \mathbf{W}^{-1} \cdot \mathbf{p}. \tag{5}$$

The real physical vector parameter $\mathbf{p}$ is easily obtained as

$$\mathbf{p} = \mathbf{W} \cdot \mathbf{p}^w. \tag{6}$$

[19] In order to obtain a stable and unique solution, we formulate the inverse problem according to regularization theory [*Tikhonov and Arsenin*, 1977] by starting with the minimization of the following objective functional

$$\phi(\mathbf{p}^w) = |\mathbf{C} \cdot (\mathbf{K}^w \cdot \mathbf{p}^w - \mathbf{d})|^2 + \alpha |\mathbf{W} \cdot \mathbf{p}^w|^2, \tag{7}$$

where $|\mathbf{C} \cdot (\mathbf{K}^w \cdot \mathbf{p}^w - \mathbf{d})|^2$ is the misfit functional responsible for data fitting, and $|\mathbf{W} \cdot \mathbf{p}^w|^2$ is a stabilizing regularization term aimed at obtaining a unique solution with the minimum length, thus reducing the dispersion of the model parameters. We assume that the noise is distributed according to a Gaussian probability distribution, so the $n \times n$ matrix $\mathbf{C}$, (whose inverse $\mathbf{C}^{-1}$ is known as the covariance matrix), is diagonal with elements σ_i^{-1}, σ_i being the standard deviation

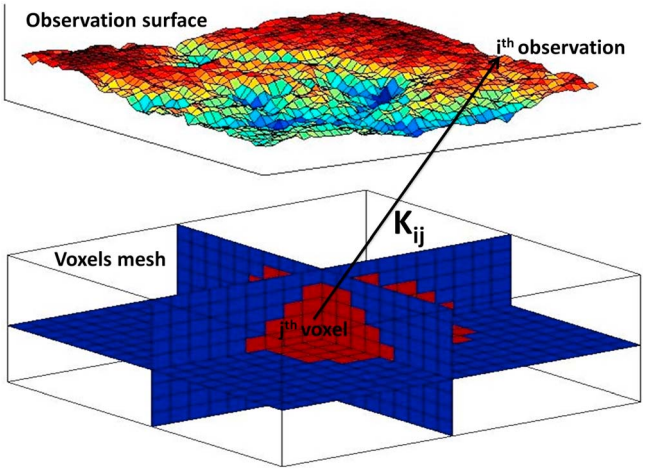

Figure 5. Example of inversion geometry and parameterization. The blue region represents everything above the bathymetry and thus is forced to be nonmagnetic.

of the ith datum. In order to obtain a focused solution showing sharp boundaries, we introduce a further regularization term in the objective functional

$$\phi(\mathbf{p}^w) = |\mathbf{C}\cdot(\mathbf{K}^w\cdot\mathbf{p}^w-\mathbf{d})|^2+\alpha|\mathbf{W}\cdot\mathbf{p}^w|^2 + \beta\sum_{j=1}^{m}\frac{\left|\nabla\left[\mathbf{W}_{jk}\mathbf{p}_k^w\right]\right|^2}{\epsilon^2+\left|\nabla\left[\mathbf{W}_{jk}\mathbf{p}_k^w\right]\right|^2}, \quad (8)$$

where we have made explicit the indexes j and k and have adapted the minimum support stabilizing functional originally introduced by *Portniaguine and Zhdanov* [2002] to the corresponding expression with the gradient operator ∇. The parameters α and β in equation (8) are Lagrange multipliers representing a reasonable compromise between data fitting and model regularization [*Tikhonov and Arsenin*, 1977]. The small factor ϵ^2 is needed to avoid singularities when $\nabla[\mathbf{W}_{jk}\mathbf{p}_k^w]=0$. The last term in equation (8) has the relevant property of minimizing the volume of the region where strong model variations occur, producing focused solutions. If we analyze in detail the expression of this term we note that it is composed of the sum of terms which may approximately exhibit values of 0 or 1. The minimization of this term consists mainly of reducing the volume of the regions where the gradient of the solution is significantly different from zero, i.e. the volume of the transitional boundary between the magnetized source and the non-magnetized background.

[20] The minimization of the functional in equation (8) proceeds by a primal-dual barrier iteration method (http://www.stanford.edu/group/sol/software/pdco.html). This method has the relevant property of allowing the user to impose lower and upper bounds for the parameter estimates by an inequality constraint. The use of this constraint reduces the instability of the inversion, especially where the solution is imposed to be only positive or negative [*Silva et al.*, 2001]. This is of particular interest in the study of magnetic anomalies where commonly we have constraints on the age of the subsurface rocks that may be relatively young whereby the corresponding magnetization may be oriented along the normal ambient geomagnetic field, i.e., positive magnetization. Moreover, the inequality constraint allows the user to introduce geological information about the rock types or the bounds on the source depth through ideal bodies approximation [*Parker*, 1974].

[21] We summarize then the inversion strategy as follows:

$$\hat{\mathbf{p}}^w = \arg\left[\min\left(|\mathbf{C}\cdot(\mathbf{K}^w\cdot\mathbf{p}^w-\mathbf{d})|^2+\alpha|\mathbf{W}\cdot\mathbf{p}^w|^2 + \beta\sum_{j=1}^{m}\frac{\left|\nabla[\mathbf{W}_{jk}\mathbf{p}_k^w]\right|^2}{\epsilon^2+\left|\nabla[\mathbf{W}_{jk}\mathbf{p}_k^w]\right|^2}\right)\right], \quad (9)$$

subject to

$$\hat{\mathbf{p}}_j^w \in \left[\mathbf{W}_{jk}^{-1}l_k, \mathbf{W}_{jk}^{-1}u_k\right], \quad (10)$$

where $\hat{\mathbf{p}}^w$ is the parameter estimate vector and l_k and u_k are the imposed lower and upper bounds on the magnetization of the k^{th} cell, respectively. The constraints expressed in the last equations provide only an approximate description of complex geologic cases. For example, the proposed method may not be accurate in the case that contacts might not be sharp, i.e., in the case of smooth boundaries. However, in the following section we show the results of the inversion program applied to some synthetic tests, that will provide the basis for the discussion of the 3-D magnetic model derived from the real data set of Brothers volcano shown in Figure 3. Our aim is to map the subsurface distribution of hydrothermal alteration at Brothers volcano, where we expect our method to be particularly effective since we expect to have sharp contacts between hydrothermally altered zones and fresh volcanic rocks.

4. Synthetic Test and Practical Tips: The Brothers Volcano Uniform Model

[22] In this section we simulate the magnetic field of a uniformly magnetized volcano to test the performance of the inversion method on a known magnetization model. To this aim, we have used the available bathymetric data for Brothers volcano (Figure 1) in the region defined by the AUV surveys (Figure 2). We have built a volcano model comprised of rocks with a constant magnetization of 5 A/m (Figure 6a) down to a flat plane at −2200 m that marks the bottom boundary of our model. The magnetic anomaly data were calculated by a 3-D FFT forward method [*Caratori Tontini et al.*, 2009; *Caratori Tontini*, 2012] at the constant observation level for the magnetic anomalies of −1100 m depth, using a magnetization direction with inclination I = −60° and declination D = 20° as the regional geomagnetic field. The corresponding anomaly map is shown in Figure 7 using a grid made up of 69 × 73 points spaced regularly at 50 m intervals. The inversion was run using a X-Y-Z mesh comprised of 69 × 73 × 21 cells, all centered under the anomaly grid and vertically extending from −1200 m, which is close to the top of the volcano, down to the bottom plane at −2200 m.

[23] The model obtained from the focused inversion is shown in Figure 6b. A qualitative comparison between this model and the synthetic model shown in Figure 6a shows a high level of similarity. Deviations from the homogeneous model are found adjacent to the edges of the source volume where the gradient constraint may fail and there are fewer neighboring magnetic data to constrain the model. For example, the inversion found a slightly reduced magnetic region inside the volcano, close to the S boundary of the caldera floor. However, the amplitude of this variation is <1 A/m, i.e., less than 20% of the magnetization value, with no significant risk to interpret this region as a non-existent altered zone. Despite being conceptually simple, this synthetic model nevertheless is a challenge for inversion based only on smoothness constraints and without focusing constraints. In Figure 6c we show the model obtained by inverting the magnetic data in Figure 7 by using the method by *Caratori Tontini et al.* [2006], which is based on a minimum-norm smooth inversion without focusing constraints. The corresponding result differs significantly from the correct distribution of magnetization (Figure 6a). For example, regions of low magnetization at the cone flanks (Figure 6c) could be interpreted erroneously as zones of alteration. The use of focusing constraints appears thus important in order to reduce this kind of ambiguity.

[24] Next we discuss some limitations of the method and some practical tips to adopt when analyzing real data, as

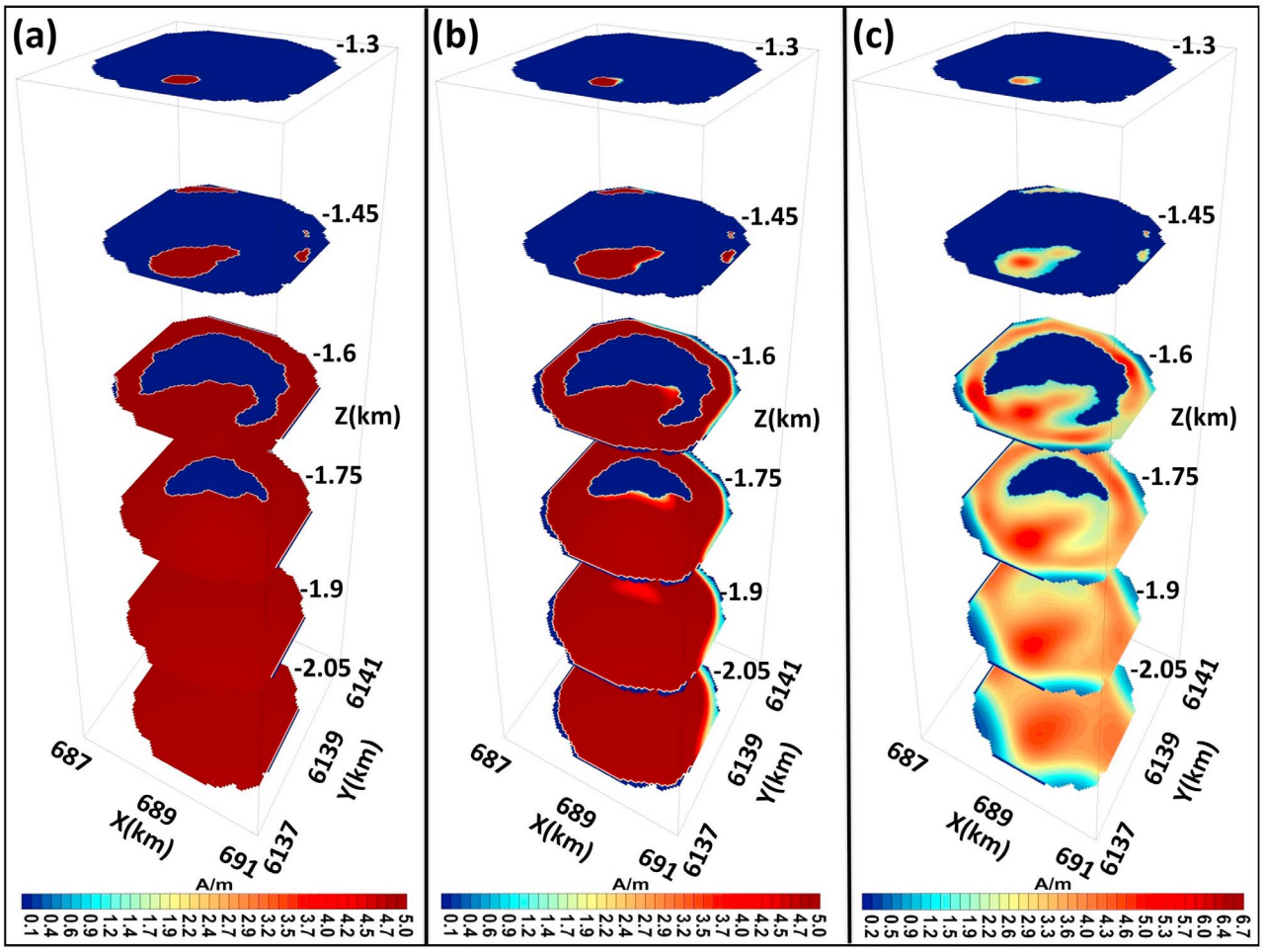

Figure 6. Synthetic test. (a) Synthetic model with uniform magnetization (5 A/m) generating the magnetic anomaly in Figure 7. (b) Inversion results by using the focusing constraints described in equation (9). (c) Minimum-norm inversion results without focusing constraints. For simplicity the model are shown by a set of 6 significant horizontal cross-sections spaced 150 m along the vertical.

some of the simplifications inherent to the synthetic tests are not valid in the case of a real magnetization distribution:

[25] 1. A well-constrained regional field has to be estimated and subtracted from the measurements [*Li and Oldenburg*, 1998]. The interpretation model is forced to lie at a given depth-interval, defined by the vertical extension of the 3-D volume that presumably is host to the source. If the signal is corrupted by a component originating from a different depth-interval, the misfit functional forces the model to reproduce the corresponding signal. This may create artifacts in the parameter estimates and the inequality constraint may fail to reproduce the observations with the required degree of accuracy;

[26] 2. The inversion program depends on the direction of the average magnetization of the rocks in terms of inclination and declination. If measurements of remanent magnetization are available from local rock samples they can be used as an input to the inversion program. Otherwise, a proper average magnetization direction can be estimated by using currently available analytical methods, [*Andersen and Pedersen*, 1979; *Phillips*, 2004; *Dannemiller and Li*, 2006; *Caratori Tontini and Pedersen*, 2008] and introduced into the inversion algorithm. Incorrect evaluation of the magnetization direction, and/or an assumption of constant magnetization direction for the source can alter the interpretation of the magnetic anomalies, providing an additional term of non-uniqueness. A well-considered estimate of the magnetization direction is therefore essential to obtain reliable results;

[27] 3. The tolerance imposed in data fitting is important for a fast convergence of the inversion program. A value for the tolerance of around 1 is recommended to solve a least squares problem once we have the correct estimate of the error on the measurements, i.e., σ_i in equation (7). If this error has been overestimated, the model anomaly can be significantly different from the measured anomaly. A proper value for the tolerance can be iteratively adjusted by running sequential inversions;

[28] 4. The inequality constraint, i.e., the imposed range of variation for the magnetization parameters, has the important property of reducing the non-uniqueness and focusing the solution. With real geological scenarios, where the magnetization is unknown, parameter ranges can be adjusted iteratively by running sequential inversions with refined magnetization

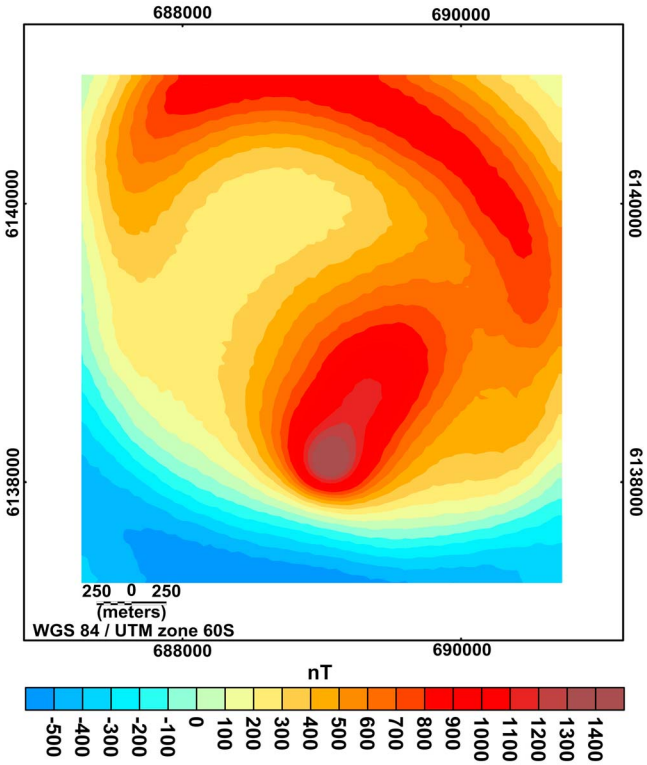

Figure 7. Synthetic magnetic anomaly generated by the uniform model in Figure 6a. Zero-mean random Gaussian noise with 30 nT standard deviation has been added to the original data to simulate a real data-set.

ranges until a reasonable compromise between data-fitting and focusing of the solution is achieved.

5. Brothers Volcano 3-D Magnetic Model: Implications for Seafloor Hydrothermal Systems

[29] In general, magnetic data provide important information regarding the subseafloor structure of submarine volcanoes and in particular, provide important constraints on the geometry of the associated hydrothermal system. This is because in these settings the rocks within the hydrothermal system are commonly altered compared to fresh volcanic rocks [*Tivey and Dyment*, 2010], which are commonly characterized by large magnetizations. By contrast, the corrosive nature of the hydrothermal fluids commonly destroys the magnetic mineral content from the host rocks, drastically reducing their magnetization, [*Johnson and Atwater*, 1977; *Rona*, 1978; *Tivey and Johnson*, 2002]. These regions of vanishing magnetization persist even if the hydrothermal field becomes extinct, making the magnetic method a powerful tool for delineating inactive hydrothermal fields. Under this assumption, we believe a focusing constraint may be particularly useful for characterizing hydrothermal alteration, where we expect sharp contacts between altered (nonmagnetic) and fresh (magnetic) rocks, rather than a smooth variation of the magnetization distribution.

[30] We show (Figures 8 and 9) the 3-D model obtained by inverting the real observations shown in Figure 3. This anomaly is based on a grid composed of 69 × 73 points regularly spaced 50 m apart. Given the close proximity of the sensor to the magnetized source, the amplitude of the anomalies and the limited extent of the survey, regional field effects are assumed to be negligible. We further assumed a magnetization direction oriented as the ambient inducing field, with inclination −60° and declination 20°, because Brothers volcano is younger than the last magnetic polarity reversal [*Malahoff et al.*, 1982]. The inversion is based on a X-Y-Z mesh made of 69 × 73 × 21 cells centered under the anomaly grid, vertically extending from −1200 m, (i.e., close to the summit of the volcano cone) down to −2200 m that marks the depth of the surrounding seafloor around the volcano. The inversion model is shown in Figure 8 by using eight relevant horizontal cross-sections spaced 100 m apart in a vertical direction, extracted from the original set of 21 horizontal sections. The morphology lineaments and the hydrothermal vent fields are also shown in this figure so that we can correlate the 3-D magnetization model with known information on the seafloor expression of hydrothermal activity at Brothers. Figure 9 shows a 3-D interpretative model by means of magnetization isosurfaces (see Figure S1 of the auxiliary material).[1]

[31] All four known hydrothermal fields at Brothers volcano are visible as vanishing magnetization regions in Figure 8. However, the horizontal slices in Figure 8 differ from the first-order 2-D inversion of *Caratori Tontini et al.* [2012] (Figure 4) because the 3-D inversion allows magnetization to vary vertically. A large volume of vanishing magnetization is found at the NW caldera site (A). As discussed by [*de Ronde et al.*, 2005, 2011], this hydrothermal field has been active for a relatively long time (≥1200 years) and is characterized by evolved seawater and magmatic fluids incorporated into the hydrothermal fluids. Here, numerous active black smoker chimneys and dead spires have been observed, representing the surface expression of focused venting. The magnetization model in Figure 8 is consistent with these observations. The vertical geometry of the low-magnetization region at the NW caldera site is significant, and extends to a depth of at least 2200 m, i.e., 400 m below the caldera floor (Figure 9a). *de Ronde et al.* [2011] have modeled the hydrothermal system at Brothers, incorporating the acoustic data of *Dziak et al.* [2008], and showed how the surface expressions of the various vent fields, and the cone (B) in particular, are likely connected to the underlying magma chamber via conduits up to 2500 m in length. This deep communication with the magma chamber has been inferred to explain the injection of magmatic volatiles into the hydrothermal fluids. Furthermore, direct communication between the vertical conduits and the magma chamber may explain the presence of high-temperature hydrothermal fluids, i.e., focused venting. The occurrence of focused venting at this site is also consistent with the deep structure of the demagnetized zone in Figure 9a, which is compatible with a vertical, pipe-like feature as observed at mid-ocean-ridge focused hydrothermal sites [*Tivey and Johnson*, 2002]. The volume of the NW caldera demagnetized zone is at least 1.2 km^3.

[32] The W caldera site (D) exhibits a similar pattern. At this site, a focused hydrothermal vent field was detected from water column anomalies measured by *ABE* [*Baker et al.*,

[1]Auxiliary materials are available in the HTML. doi:10.1029/2012JB009349.

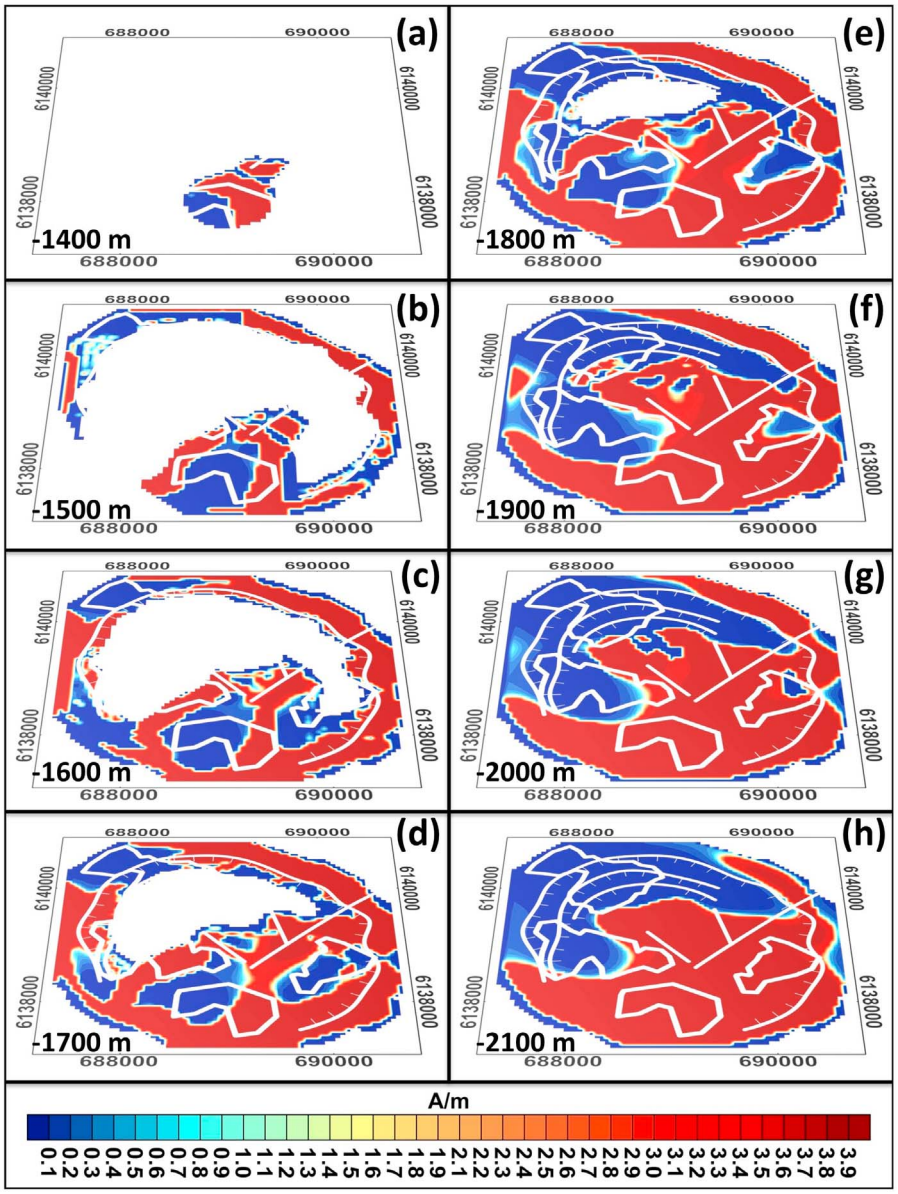

Figure 8. Brothers volcano magnetization model from *ABE* and *Sentry* observations shown in Figure 3. The magnetization model has been clipped by the topography (white areas). The blue areas indicate low-magnetization regions (0 A/m) correlated with the hydrothermal system. The model is shown by a set of eight significant horizontal cross-sections spaced 100 m along the vertical.

2012] and by a single dive made by the ROV *Quest6000* during the 2007 ROVARK cruise. The subsurface expression of the magnetization distribution is characterized by a vertical demagnetized conduit extending down to at least 2200 m depth (Figure 9d). Whereas the shallow magnetic signatures of the NW and West caldera fields are distinct and are separated by a highly magnetized structure (Figures 8c–8e), at depths greater than 1900 m (Figure 8e), i.e., immediately below the caldera floor at ~1850 m, the two demagnetization regions merge and then coalesce into a single, broader demagnetized region. According to *Dziak et al.* [2008], at depths about 2200 m, i.e., 400 m below the caldera floor, the hydrothermal system is undergoing gas explosions and generating significant tremor, indicating a boiling phase separation. At these pressures, this phase transition may indicate temperature in the range 300°–400°.

[33] The broad demagnetized region below the caldera floor could then be explained as a result of thermal demagnetization, since the Curie temperature for titanomagnetite can be as low as 260°. However, the arcuate shape along the caldera walls, suggests that large-scale permeability variations associated with the ring faults may play a relevant role in the hydrothermal fluids circulation. The vertical shape of the W caldera site is again compatible with a pipe-like structure (Figure 9d), but in this case the volume of the corresponding upflow zone is about 0.6 km^3, ~half of the NW site volume. Thus, the magnetic signature of this site appears to be compatible with that of a smaller focused site.

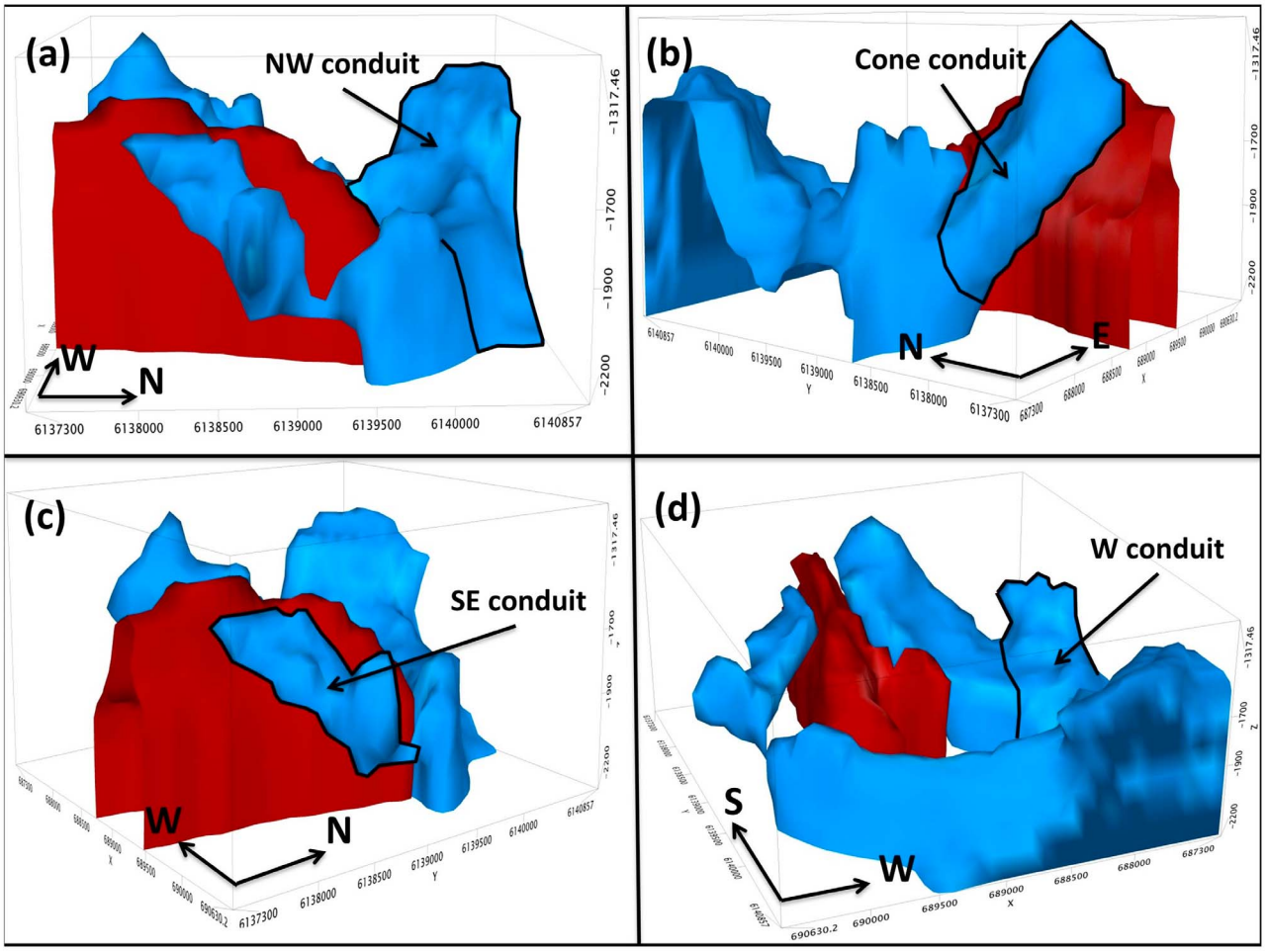

Figure 9. Brothers volcano 3-D model by magnetization isosurfaces. The isosurfaces colors are based on the color mapping of Figure 8, i.e., the blue isosurface highlights low-magnetization upflow zones whereas the red isosurface shows the magnetized central dike (Figure 1). (a–d) Each perspective view is oriented to show a particular hydrothermal site in detail.

[34] The cone site (B) and the East caldera site (C) have different magnetization signatures (Figures 9b and 9c) in comparison with the focused NW caldera and W caldera sites (Figures 9a–9d). Differences in the magnetization pattern between focused (A, D) and diffuse (B, C) vent sites at Brothers are discussed in *Caratori Tontini et al.* [2012], and can be summarized here by noting that the amplitudes of the low-magnetization anomalies appear more intense at focused sites than at diffuse sites (Figure 4). The possible causes were attributed to variations in the thickness of the demagnetized layer and/or the duration of hydrothermal activity and consequent destruction of magnetic minerals [*Caratori Tontini et al.*, 2012]. However, due to the lack of depth resolution of the 2-D inversion, both interpretations were considered possible. Our 3-D magnetization model, however, provides evidence that the vertical extent of the demagnetized conduits at the diffuse (low-temperature) sites is less than the corresponding conduits at focused sites. It is possible that the hydrothermal fluid upflow at the diffuse venting sites (especially at the Cone site) may be supplied at greater depths by fluids moving laterally from the adjacent focused vent sites conduits. Distinct, linear, high-magnetization features separate the shallow portion of each of the four hydrothermal vent fields, while the deeper parts of the demagnetized conduits below the diffuse venting sites appear to migrate toward the focused vent sites conduits (Figures 9b and 9c). The geometry of the demagnetized zones below focused vent sites resembles vertical pipe-like structures. By contrast, where diffuse venting occurs at the Cone and SE caldera sites, the corresponding demagnetized zones have cylinder-shaped geometries that dip northward (Figures 9b and 9c). The deep connection between these inclined upflow zones at the diffuse sites is particularly evident in Figure 9b, where the Cone site upflow zone coalesces with the deep root of the W caldera site upflow zone at depths greater than ~1800 m. This deep connection may explain the presence of magmatic fluids into the hydrothermal fluids [*de Ronde et al.*, 2011], particularly at the cone site. Also, the volumes of the demagnetized conduits at diffuse sites are smaller than the NW caldera site, being 0.7 km^3 and 0.4 km^3 at the Cone site and SE caldera site, respectively.

[35] Another important structure that shows a clear magnetization signature is the dike-like magnetized body that parallels the cone alignment. This is marked as a SW-NE line in Figures 1 and 8, and corresponds to morphological

evidence of a dike being emplaced in this region at Brothers volcano [*de Ronde et al.*, 2005]. The magnetization signature of this dike was discussed by *Caratori Tontini et al.* [2012] as a structural feature separating the W caldera site from the SE caldera site (Figure 4). The 3-D representation of Figure 9 clearly shows that the magnetization expression of this body (i.e., the red isosurface) is compatible with a tabular shape characteristic of a dike. This structure acts as a boundary between the SE and Cone site conduits. The dike emplacement may have acted as a permeability barrier, splitting the pre-existing hydrothermal field into two separate conduits with the cone site and SE caldera site surface manifestations, interrupting the deep connection between the SE caldera site and the magma chamber. This may explain the injection of more magmatic volatiles into the hydrothermal fluids at the cone site.

6. Conclusion

[36] We have shown results of applying a 3-D inversion algorithm for magnetic data, with the aim of obtaining a focused solution within a predetermined range of magnetization amplitudes and assuming knowledge of the causative body's top and bottom surface. The method has been tested on a submarine volcano synthetic model that provided realistic results. We have then applied the algorithm to real, near-bottom magnetic data acquired by AUVs over the submarine Brothers volcano. The resulting magnetic model provides important results regarding the geometry of subseafloor upflow zones beneath different seafloor manifestations of venting, i.e., focused versus diffuse venting, and the corresponding magnetization distributions. Focused venting is characterized by nearly vertical, pipe-like upflow zones whereas at diffuse venting the vertical extension of the demagnetized region is inclined and limited to the shallow subsurface. This method, when combined with other methods, such as hydrothermal plume mapping, that can detect active venting, becomes an essential tool in the exploration of seafloor hydrothermal systems. We believe that the 3-D inversion method described here is suitable for a variety of geological models in addition to volcano-hosted submarine hydrothermal systems.

[37] **Acknowledgments.** The paper has greatly benefited from the review by Richard J. Blakely and discussions with Jerome Dyment and Florent Szitkar. We acknowledge the crews and captains of both the R/V *Sonne* and R/V *Tangaroa* for safe deployment and recovery of the *ABE* and *Sentry* vehicles. We also acknowledge Andy Billings, Alan Duester and Carl Kaiser from WHOI who successfully operated *ABE* and *Sentry*. This contribution was made possible through funding by the New Zealand Foundation for Research, Science and Technology (FRST contract C05X0406) and by the Royal Society of New Zealand by the Marsden Fund (grant GNS1003).

References

Andersen, F. H., and L. B. Pedersen (1979), Some relations between potential fields and the strength and center of their sources, *Geophys. Prospect.*, *27*, 761–774.

Baker, E. T., R. W. Embley, C. E. J. de Ronde, and S. Walker (2012), High-resolution hydrothermal mapping of Brothers caldera, Kermadec arc, *Econ. Geol.*, in press.

Barbosa, V. C. F., and J. B. C. Silva (1994), Generalized compact gravity inversion, *Geophysics*, *59*, 57–68.

Bhattacharyya, B. K. (1964), Magnetic anomalies due to prism-shaped bodies with arbitrary polarization, *Geophysics*, *29*, 517–531.

Blakely, R. J. (1995), *Potential Theory in Gravity and Magnetic Applications*, Cambridge Univ. Press, New York.

Boulanger, O., and M. Chouteau (2001), Constraints in 3D gravity inversion, *Geophys. Prospect.*, *49*, 265–280.

Caratori Tontini, F. (2012), Rapid interactive modeling of 3-D magnetic anomalies, *Comput. Geosci.*, *48*, 308–315, doi:10.1016/j.cageo.2012.01.006.

Caratori Tontini, F., and L. B. Pedersen (2008), Interpreting magnetic data by integral moments, *Geophys. J. Int.*, *174*, 815–824.

Caratori Tontini, F., O. Faggioni, N. Beverini, and C. Carmisciano (2003), Gaussian envelope for 3D geomagnetic data inversion, *Geophysics*, *68*, 996–1007.

Caratori Tontini, F., L. Cocchi, and C. Carmisciano (2006), Depth-to-the-bottom optimization for magnetic data inversion: Magnetic structure of the Latium volcanic region, Italy, *J. Geophys. Res.*, *111*, B11104, doi:10.1029/2005JB004109.

Caratori Tontini, F., L. Cocchi, and C. Carmisciano (2009), Rapid 3-D forward model of potential fields with application to the Palinuro Seamount magnetic anomaly (southern Tyrrheania Sea, Italy), *J. Geophys. Res.*, *114*, B02103, doi:10.1029/2008JB005907.

Caratori Tontini, F., L. Cocchi, F. Muccini, C. Carmisciano, M. Marani, E. Bonatti, M. Ligi, and E. Boschi (2010), Potential-field modeling of collapse-prone submarine volcanoes in the southern Tyrrhenian Sea (Italy), *Geophys. Res. Lett.*, *37*, L03305, doi:10.1029/2009GL041757.

Caratori Tontini, F., B. Davy, C. E. J. de Ronde, R. W. Embley, M. Leybourne, and M. A. Tivey (2012), Crustal magnetization of Brothers volcano, New Zealand, measured by autonomous underwater vehicles: Geophysical expression of a submarine hydrothermal system, *Econ. Geol.*, in press.

Cella, F., and M. Fedi (2012), Inversion of potential field data using the structural index as weighting function rate decay, *Geophys. Prospect.*, *60*, 313–336.

Cocchi, L., F. Caratori Tontini, F. Muccini, M. P. Marani, G. Bortoluzzi, and C. Carmisciano (2009), Chronology of the transition from a spreading ridge to an accretional seamount in the Marsili backarc basin (Tyrrhenian Sea), *Terra Nova*, *21*, 369–374.

Dannemiller, N., and Y. Li (2006), A new method for determination of magnetization direction, *Geophysics*, *71*, L69–L73.

DeMets, C., R. G. Gordon, and D. F. Argus (2010), Geologically current plate motions, *Geophys. J. Int.*, *181*, 1–80.

de Ronde, C. E. J., E. T. Baker, G. J. Massoth, L. E. Lupton, I. C. Wright, R. A. Feely, and R. G. Greene (2001), Intra-oceanic subduction-related hydrothermal venting, Kermadec volcanic arc, New Zealand, *Earth Planet. Sci. Lett.*, *193*, 359–369.

de Ronde, C. E. J., et al. (2005), Evolution of a submarine magmatic-hydrothermal system: Brothers volcano, southern Kermadec Arc, New Zealand, *Econ. Geol.*, *100*, 1097–1133.

de Ronde, C. E. J., et al. (2007), Submarine hydrothermal activity along the mid-Kermadec Arc, New Zealand: Large-scale effects on venting, *Geochem. Geophys. Geosyst.*, *8*, Q07007, doi:10.1029/2006GC001495.

de Ronde, C. E. J., et al. (2011), Submarine hydrothermal activity and gold-rich mineralization at Brothers volcano, Kermadec arc, New Zealand, *Miner. Deposita*, *46*, 541–584, doi:10.1007/s00126-011-0345-8.

Dziak, R. P., J. H. Haxel, H. Matsumoto, T. K. Lau, S. G. Merle, C. E. J. de Ronde, R. W. Embley, and D. K. Mellinger (2008), Observations of regional seismicity and local harmonic tremor at Brothers volcano, south Kermadec arc, using an ocean bottom hydrophone array, *J. Geophys. Res.*, *113*, B08S04, doi:10.1029/2007JB005533.

Embley, R. W., C. E. J. de Ronde, F. C. Tontini, B. Davy, E. T. Baker, and D. Yoerger (2012), Detailed morphology and structure of an active submarine arc caldera: Brothers volcano, Kermadec arc, *Econ. Geol.*, in press.

Faggioni, O., and F. Caratori Tontini (2003), Quantitative evaluation of the time-line reduction performance in high definition marine magnetic surveys, *Mar. Geophys. Res.*, *23*, 353–365.

Finlay, C. C., et al. (2010), International geomagnetic reference field: The eleventh generation, *Geophys. J. Int.*, *183*, 1216–1230.

Guillen, A., and V. Menichetti (1984), Gravity and magnetic inversion with minimization of a specific functional, *Geophysics*, *49*, 1354–1360.

Ho-Liu, P., J.-P. Montagner, and H. Kanamori (1989), Comparison of iterative back-projection inversion and generalized inversion without blocks: Case studies in attenuation tomography, *Geophys. J. Int.*, *97*, 19–29.

Johnson, H. P., and T. Atwater (1977), Magnetic study of basalts from the Mid-Atlantic ridge, lat. 37°N, *Geol. Soc. Am. Bull.*, *88*, 637–647.

Last, B. J., and K. Kubik (1983), Compact gravity inversion, *Geophysics*, *48*, 713–721.

Li, Y., and D. W. Oldenburg (1996), 3-D inversion of magnetic data, *Geophysics*, *61*, 394–408.

Li, Y., and D. W. Oldenburg (1998), Separation of regional and residual magnetic field data, *Geophysics*, *63*, 431–439.

Malahoff, A., R. H. Feden, and H. S. Fleming (1982), Magnetic anomalies and tectonic fabric of marginal basins north of New Zealand, *J. Geophys. Res.*, *87*, 4109–4125.

Menke, W. (1989), *Geophysical Data Analysis: Discrete Inverse Theory*, Elsevier, New York.

Merle, S., et al. (2007), New Zealand American Submarine Ring of Fire 2007 Cruise Report, report, Natl. Oceanic and Atmos. Admin., Washington, D. C.

Parker, R. L. (1974), Best bounds on density and depth from gravity data, *Geophysics*, *39*, 644–649.

Parker, R. L., and S. P. Huestis (1974), The inversion of magnetic anomalies in the presence of topography, *J. Geophys. Res.*, *79*, 1587–1593.

Phillips, J. D. (2004), Can we estimate total magnetization directions from aeromagnetic data using Helbig's integrals?, *Earth Planets Space*, *57*, 681–689.

Pilkington, M. (1997), 3-D magnetic imaging using conjugate gradients, *Geophysics*, *62*, 1132–1142.

Portniaguine, O., and M. S. Zhdanov (2002), 3-D magnetic inversion with data compression and image focusing, *Geophysics*, *67*, 1532–1541.

Rona, P. A. (1978), Magnetic signatures of hydrothermal alteration and volcanogenic mineral deposits in oceanic crust, *J. Volcanol. Geotherm. Res.*, *3*, 219–225.

Silva, J. B. C., W. E. Medeiros, and V. C. F. Barbosa (2001), Potential-field inversion: Choosing the appropriate technique to solve a geological problem, *Geophysics*, *66*, 511–520.

Simons, F. J., R. D. van der Hilst, J.-P. Montagner, and A. Zielhuis (2002), Multimode Rayleigh wave inversion for heterogeneity and azimuthal anisotropy of the Australian upper mantle, *Geophys. J. Int.*, *151*, 738–754.

Tarantola, A. (1987), *Inverse Problem Theory*, Elsevier, New York.

Tikhonov, A. N., and V. Y. Arsenin (1977), *Solutions of Ill-Posed Problems*, Winston, Washington, D. C.

Tivey, M. A., and J. Dyment (2010), The magnetic signature of hydrothermal systems in slow spreading environments, in *Diversity of Hydrothermal Systems on Slow Spreading Ocean Ridges*, *Geophys. Monogr. Ser.*, vol. 188, edited by P. Rona, C. Devey, and B. Murton, pp. 43–65, AGU, Washington, D. C.

Tivey, M. A., and H. P. Johnson (2002), Crustal magnetization reveals subsurface structure of Juan de Fuca Ridge hydrothermal vent fields, *Geology*, *30*, 979–982.

Tivey, M. A., H. Schouten, and M. C. Kleinrock (2003), A near-bottom magnetic survey of the Mid-Atlantic Ridge axis at 26°N: Implications for the tectonic evolution of the TAG segment, *J. Geophys. Res.*, *108*(B5), 2277, doi:10.1029/2002JB001967.

Wright, I. C. (1994), Nature and tectonic setting of the southern Kermadec submarine arc volcanoes: An overview, *Mar. Geol.*, *118*, 217–236.

Wright, I. C., C. E. J. de Ronde, K. Faure, and J. A. Gamble (1998), Discovery of hydrothermal sulfide mineralization from southern Kermadec arc volcanoes (SW Pacific), *Earth Planet. Sci. Lett.*, *164*, 334–343.

Yanovskaya, T. B., and P. G. Ditmar (1990), Smoothness criteria in surface wave tomography, *Geophys. J. Int.*, *102*, 63–72.

Zhdanov, M. (2002), *Geophysical Inverse Theory and Regularization Problems*, Elsevier, Amsterdam.